Global Sensitivity Analysis of Aging Parameters for a Lithium-ion Battery Cell using Optimal Charging Profiles

Muhammad Aadil Khan[1], Vahid Azimi[2], and Simona Onori[2]

Abstract— A challenge with Lithium-ion battery (LIB) cells is to study the impact of degradation parameter variations on the model outputs. These parameters not only contribute to battery aging, but also their accurate identification is crucial to enhance battery management systems design. This paper employs a global sensitivity analysis technique to analyze the impact of kinetic, design, and solid-electrolyte interphase (SEI) aging parameters on two different outputs, i.e., cell voltage and charge capacity. The cell is modeled via a coupled nonlinear partial and ordinary differential equations, and differential algebraic equations representing the electrochemical, thermal, and aging dynamics of a LIB cell via the enhanced single particle model (ESPM). To perform the analysis, we adopt different optimal currents at three ambient temperatures to achieve fast charging-minimum degradation profiles. The analysis shows that anode active phase volume fraction, anode reaction rate constant, and solvent reduction kinetic constant are the most sensitive parameters for both outputs.

Index Terms— Lithium-ion battery, Enhanced single particle model, Aging, Global sensitivity analysis.

I. INTRODUCTION

Over the last decade, the use of lithium-ion battery (LIB) has increased manifolds as the world moves towards sustainable energy resources instead of fossil fuels. In 2017, electric vehicles (EVs) surpassed global sales of one million units. This global transition towards EVs has increased the importance of developing battery management systems (BMSs) that can not only inform the user about battery diagnostics, but also ensure a high-level of performance. Different kinds of battery models have been developed by researchers such as models based on circuit designs [1] using resistors and capacitors, or physics-based/electrochemical models like Pseudo-two-Dimensional (P2D) [2] based on porous electrode theory. The latter models are complex, but provide great insights into the behavior of an actual battery. Sensitivity Analysis (SA) determines how variation in the model parameters affects the output of the model. Some parameters of the model are generally more sensitive than others. Since electrochemical models for LIBs contain a large number of parameters, it is helpful to know which parameters cause a significant variation in the output(s) of the model. These highly sensitive parameters are the ones that have to be accurately estimated for the model to perform accurately. In [3], one-factor-at-a-time sensitivity analysis is performed for an Equivalent Circuit Model (ECM) and a reduced-order model was developed using the sensitive parameters. In [4] combined electrochemical impedance spectroscopy with machine learning, and used systematic parameter sensitivity analysis to identify parameters that are important for battery screening and health diagnosis. A Kriging-based global sensitivity analysis (GSA) was performed in [5] to study parameters that cause thermal variations. Since it is important to verify SA in practical scenarios, the work in [6] used real-world driving cycles on an electrochemical model of lithium cells to conduct a local sensitivity analysis. In that work, in addition to the terminal voltage, essential states of the model, e.g., cathode bulk state of charge, cathode surface state of charge, and anode potential, were also considered as outputs. Similarly, L_2-norm-based local sensitivity analysis was conducted in [7] where the effect of input parameters was checked with respect to specific capacity of Li-O_2 batteries. In [8], sensitivity analysis for multi-physics model of graphite/LiFePO$_4$ battery was performed under different conditions, e.g., temperature, discharge rate, etc. Many global sensitivity analyses are performed through Monte Carlo simulations. The work done in [9] builds a probabilistic framework through a Gaussian process emulator that mitigates the high dimensionality of the problem. This allowed a SA to be performed using Monte Carlo sampling for multi-output problems and also provided error bounds for different sensitivity measures. A common technique in GSA is Morris' screening method [10] that uses mean and standard deviation to recognize parameters that are sensitive and/or have a large number of interactions with other parameters. In [11], the Point Estimate Method (PEM) was used for its low computational effort to conduct GSA on Single Particle Model with electrolyte and thermal dynamics. Despite the rich literature on using SA on electrochemical models for LIBs, there is a current gap in understanding the sensitivity of aging parameters towards various outputs of the model. The novel contributions of this paper include: i) the use of Morris' screening method on an electrochemical-thermal-aging model, ii) studying the sensitivity of the aging parameters for the cell voltage and capacity over optimized current charging profiles. Seven aging parameters are included in the sensitivity analysis. The results are generated for nine different optimal charging current profiles at ambient temperatures of $15°C$, $25°C$, and $35°C$. Results show that anode solid phase volume fraction, anode reaction rate constant, and solvent reduction kinetic constant have the most impact on the model outputs, i.e., cell voltage and capacity.

Notations: The following notations are used: $\mathbf{x}$ =

---

[1]M. A. Khan is with the Department of Mechanical Engineering, Stanford University, CA 94305, USA `maadilk@stanford.edu`

[2]V. Azimi and S. Onori are with the Department of Energy Resources Engineering, Stanford University, CA 94305, USA `vazimi@stanford.edu, sonori@stanford.edu`

234

$[x_1, \ldots, x_n]^T \in \mathbb{R}^n$ is a vector of parameters, $\mathbf{A} \in \mathbb{R}^{m \times n}$ is a matrix of dimensions m-by-n, and $|.|$ denotes the absolute value of a scaler variable. Subscript j denotes the domain in the lithium-ion battery. In the solid phase, it denotes the negative and positive electrode, j∈[n,p], whereas, in the electrolyte phase, it represents the negative electrode, separator, and positive electrode, j∈[n,s,p].

II. CELL MODEL EQUATIONS

The dynamics of a LIB cell are complex and coupled through non-linear ODEs, PDEs, and DAEs. Each electrode in the ESPM is approximated as a single spherical particle withh uniform current density. Eq. (1), (2), and (3) are PDEs describing the electrochemical dynamics of the cell. The surface overpotentials η_j, described by Eq. (4), are calculated for each electrode intercalation reaction using electrode surface and averaged electrolyte concentration of each domain assuming Butler-Volmer kinetics. Eq. (5) describes the exchange current density $i_{0,j}$. To compute the open circuit potentials U_j, empirical relationships are used that are based on electrode surface concentration stoichiometry [13]. Finally, the voltage of the cell can be computed using Eq. (6). The ohmic resistance of the cell is divided into Solid Electrolyte Interphase (SEI) layer resistance R_{sei}, lumped contact resistance R_l, and electrolyte resistance R_{el}. From [14], SEI and electrolyte resistances are given by

$$R_{sei} = \frac{L_{sei}}{a_{s,n} A L_n \kappa_{sei}} \tag{13}$$

$$R_{el} = \frac{1}{2A} \left[\frac{L_n}{\kappa_{e,n}^{eff}} + \frac{2L_s}{\kappa_{e,s}^{eff}} + \frac{L_p}{\kappa_{e,p}^{eff}} \right] \tag{14}$$

where $\kappa_{e,j}^{eff} = f(c_{e,j}^{avg}, \epsilon_{e,j})$ and $c_{e,j}^{avg}$ is the average concentration in the electrolyte phase. To model the temperature of a cell, the two-state thermal model using a lumped parameter [15] is used. The two temperatures considered are the core temperature T_c and the surface temperature T_s expressed in Eq. (7) and (8) respectively. Electrode overpotentials and Joule heating are the main sources of heat generation inside the cell while the entropic contributions are assumed negligible. In this model, aging is based on the growth of SEI layer as a function of both solvent reduction kinetics and diffusion dynamics, which is used to predict the cell capacity loss and power fade [14] [16]. Eq. (9) describes the solvent concentration available for reduction reaction at the anode surface. SEI layer growth is modeled as linearly related to the side-reaction current density i_s in Eq. (10), and i_s is defined by Eq. (11). For capacity loss, the side reaction current is integrated across the anode active surface area through Eq. (12). This amounts to the lithium content consumed by the solvent reduction reaction. At the same time, anode porosity $\epsilon_{e,n}$ changes based on the change in the SEI layer thickness according to the volume balance approach given by [14]

$$\epsilon_{e,n} = 1 - \epsilon_{s,n} \left(1 + \frac{3L_{sei}}{R_{s,n}} \right) - \epsilon_{f,n} \tag{15}$$

For robust model performance, concentration and temperature-dependent transport and kinetic parameters are updated at each point in time based on the relevant state. Empirical relationships for temperature and concentration dependencies of electrolyte parameters $D_{e,j}$ and $\kappa_{e,j}$ are found in [17]. Similarly, solid electrode parameters like $D_{s,j}$ and k_j follow an Arrhenius relationship with temperature [12]. The parameter identification and the model implementationconducted in [21] are used in this work. [22]. Parameter sensitivity analysis helps to identify the influence of model parameters on the output of the system. Not all parameters have an equal affect on the output. In the next section, Morris method is implemented to separate high influence parameters from low influence parameters on the chosen outputs. Morris' method [18] is a commonly-used technique for sensitivity analysis of a mathematical model characterized by a large number of parameters over which is performs a screening to separate out the most from the least sensitive parameters. The nominal parameter vector is defined as $\mathbf{x}^* = [x_1, x_2, \ldots, x_k] \in \Omega$ where each x_i is rescaled between $[0, 1]$, and k is the number of parameters. This input space is divided into equally-sized intervals or levels which is denoted by p. Common values of p are 4 or 10. During analysis, each parameter is multiplied by its nominal value to use the right value in the model. The complete input space becomes a k-dimensional p-level grid denoted by $\Omega \in \mathbb{R}^{k \times p}$. One of the k parameters is randomly selected from $\mathbf{x}^*$ and its value is increased or decreased by Δ such that

$$\mathbf{x}^{(1)} = (x_1, \ldots, x_{i-1}, x_i \pm \Delta_i, x_{i+1}, \ldots, x_k) \in \Omega \tag{16}$$

where $\Delta = p/2(p-1)$ [18]. Once the perturbed parameter vector is obtained, elementary effect is computed for the ith parameter $\xi_i = \frac{y(\mathbf{x}^{(1)}) - y(\mathbf{x}^*)}{\pm \Delta_i}$ where $i = 1, \ldots, k$. This step is repeated for all parameters $j \neq i$, and afterwards, the complete experiment is repeated r times which results in extensive exploration of the input space. Once all the elementary effects ξ_i have been computed, the mean and standard deviation of the elementary effects are defined as follows.

$$\mu_i = \frac{1}{r} \sum_{j=1}^{r} \xi_i \left(x^{(j)} \right) \tag{17}$$

$$\mu_i^* = \frac{1}{r} \sum_{j=1}^{r} \left| \xi_i(x^{(j)}) \right| \tag{18}$$

$$\sigma_i = \sqrt{\frac{1}{r-1} \sum_{j=1}^{r} \left(\xi_i \left(x^{(j)} \right) - \mu_i \right)^2} \tag{19}$$

where r is the number of times the experiment is performed. Usually, elementary effects can assume both signs and cancel each other out. To avoid this, the absolute value of the elementary effects is used and the mean is denoted by μ^* as shown in Eq. (18). The parameters that have a high mean have a greater overall impact on the output while parameters with a high standard deviation have a more non-linear relationship with the output and/or have interactions with other parameters. A technical

TABLE I: Electrochemical-thermal-aging dynamics of a LIB cell.

Electrochemical dynamics [19]		
Mass conservation in solid phase	$\dfrac{\partial c_{s,j}}{\partial t} = \dfrac{D_{s,j}(T)}{r^2} \dfrac{\partial}{\partial r}\left[r^2 \dfrac{\partial c_{s,j}}{\partial r}\right], \qquad j \in [n,p]$	(1)
	$\left.\dfrac{\partial c_{s,j}}{\partial r}\right|_{r=0} = 0 \quad \left.\dfrac{\partial c_{s,j}}{\partial r}\right|_{r=R_{s,j}} = \dfrac{\pm I_{app}}{D_{s,j}(T)a_{s,j}AL_jF} + g_{s,j}(c_{s,j}^{surf}, c_{solv}^{surf}, T_c, I_{app}, L_{sei})$	
Mass conservation in electrolyte phase	$\epsilon_{e,j}\dfrac{\partial c_e}{\partial t} = \dfrac{\partial}{\partial x}\left(D_{e,j}^{eff}(c_e,T)\dfrac{\partial c_e}{\partial x}\right) + \left(1 - t_0^+\right)\dfrac{g_{e,j}I_{app}}{AL_jF}, \qquad j \in [n,s,p]$	(2)
	$\left.\dfrac{\partial c_e}{\partial x}\right|_{x=0} = \left.\dfrac{\partial c_e}{\partial x}\right|_{x=L_n+L_s+L_p} = 0$	
	$D_{e,n}^{eff}(c_e,T)\left(\dfrac{\partial c_e}{\partial x}(x,t)\right)\Big|_{x=L_n} = D_{e,s}^{eff}(c_e,T)\left(\dfrac{\partial c_e}{\partial x}(x,t)\right)\Big|_{x=L_n}$	
	$D_e^{eff}(c_e,T)\left(\dfrac{\partial c_e}{\partial x}(x,t)\right)\Big|_{x=L_n+L_s} = D_e^{eff}(c_e,T)\left(\dfrac{\partial c_e}{\partial x}(x,t)\right)\Big|_{x=L_n+L_s}$	
Charge conservation in electrolyte phase	$\kappa_{e,j}^{eff}(c_e,T)\dfrac{\partial^2 \Phi_e}{\partial x^2} - \kappa_D^{eff}(c_e,T)\dfrac{\partial^2 \ln c_e}{\partial x^2} + \dfrac{I_{app}}{a_{s,j}AL_j} = 0, \qquad j \in [n,s,p]$	(3)
	$\left.\dfrac{\partial \Phi_e}{\partial x}\right|_{x=0} = \left.\dfrac{\partial \Phi_e}{\partial x}\right|_{x=L_n+L_s+L_p} = 0$	
Electrode Overpotential	$\eta_j = \dfrac{R_gT_c}{0.5F} sinh^{-1}\left(\dfrac{I_{app}}{2Aa_{s,j}L_ji_{0,j}}\right), \qquad j \in [n,p]$	(4)
Exchange Current Density	$i_{0,j} = k_jF\sqrt{c_{e,j}^{avg}c_{s,j}^{surf}\left(c_{s,j}^{max} - c_{s,j}^{surf}\right)}, \qquad j \in [n,p]$	(5)
Cell voltage	$V_{cell} = U_p + \eta_p - U_n - \eta_n + \Delta\Phi_e - I_{app}(R_l + R_{el} + R_{sei})$	(6)
Thermal dynamics [15]		
Cell Core Heat Balance	$C_c\dfrac{dT_c}{dt} = I_{app}(V_{oc} - V_{cell}) + \dfrac{T_s - T_c}{R_c}$	(7)
Cell Surface Heat Balance	$C_s\dfrac{dT_s}{dt} = \dfrac{T_{amb} - T_s}{R_u} - \dfrac{T_s - T_c}{R_c}$	(8)
Aging dynamics [14] [16]		
Mass conservation in SEI	$\dfrac{\partial c_{solv}}{\partial t} = D_{solv}(T)\dfrac{\partial^2 c_{solv}}{\partial r^2} - \dfrac{dL_{sei}}{dt}\dfrac{\partial c_{solv}}{\partial r},$	(9)
	$-D_{solv}(T)\dfrac{\partial c_{solv}}{\partial r}\Big|_{r=R_{s,n}} + \dfrac{dL_{sei}}{dt}c_{solv}^{surf} = \dfrac{i_s}{F}$	
	$c_{solv}\Big|_{r=R_n+L_{sei}} = \epsilon_{sei}c_{solv}^{bulk}$	
SEI layer growth	$\dfrac{dL_{sei}}{dt} = -\dfrac{i_sM_{sei}}{2F\rho_{sei}},$	(10)
Side reaction current density	$i_s = -2Fk_f(c_{s,n}^{surf})^2 c_{solv}^{surf}\exp\left[\dfrac{-\beta F}{R_gT_c}(\Phi_{s,n} - R_{sei}I_{app} - U_s)\right]$	(11)
Cell capacity loss	$\dfrac{dQ}{dt} = i_sAL_na_{s,n}$	(12)

framework exists to generate trajectories with the desired properties in the form of the matrix $\mathbf{B}^* \in \mathbb{R}^{(k+1)\times k}$ where the rows of $\mathbf{B}^*$ are $x_1, x_2, \ldots, x_{(k+1)}$. The randomized version of the sampling matrix $\mathbf{B}^*$ is given by $\mathbf{B}^* = \left(\mathbf{J}_{k+1,1}\mathbf{x}^* + (\Delta/2)[(2\mathbf{B} - \mathbf{J}_{k+1,k})\mathbf{D}^* + \mathbf{J}_{k+1,k}]\right)\mathbf{P}^*$ where $\mathbf{B}$ is a strictly lower triangular matrix of ones and $\mathbf{J}_{k+1,k}$ is a $(k+1)\times k$ dimensional matrix of ones, $\mathbf{D}^*$ is a k-dimensional diagonal matrix with either minus one or plus one on the diagonal with equal probability, $\mathbf{P}^*$ is a k-dimensional square permutation matrix with one element equal to one in each row and remaining elements equal to zero, and $\mathbf{x}^*$ is a randomly-chosen base vector from the input space Ω.

III. RESULTS & DISCUSSION

The focus of this work is to find out the impact of aging parameter variations on voltage and capacity. To extract these parameters, the chain of electrochemical equations for both voltage and capacity is studied. To analyze the cell voltage (Eq. (6)), anode overpotential η_n (Eq. (4)) is considered

from which the only state-varying parameter is exchange current density $i_{0,n}$. In view of Eq. (5), the anode reaction rate constant k_n is a parameter that varies over aging. The R_{sei} and R_{el}, defined by Eq. (13) and (14) are a function of the aging parameters SEI layer ionic conductivity κ_{sei} and anode solid phase volume fraction $\epsilon_{s,n}$. The rate of change of capacity, Eq. (12), is linearly dependent on i_s (Eq. (11)) from which the solvent reduction kinetic constant k_f is one parameter that affects capacity. Furthermore, i_s is also related to the rate of change of L_{sei} (Eq. (10)) which contains SEI layer density ρ_{sei} that varies with aging. i_s also contains anode surface potential $\phi_{s,n}$ defined as

$$\phi_{s,n} = U_n + \eta_n + \frac{L_{sei}I_{app}}{a_{s,n}AL_n\kappa_{sei}} \tag{20}$$

Since Eq. (20) contains η_n, we can conclude that k_n affects the capacity as well. Apart from these parameters, we also include anode particle radius $R_{s,n}$ and anode diffusion coefficient $D_{s,n}$ in our analysis due to their indirect impact

on the outputs. Table II shows the parameters with their nominal values. For running Morris' method, we set the number of experiments to $r = 4$, which implies that a total of $r(k + 1)$ simulations are run to get the final results. The level for the input space Ω is set to $p = 4$. For each parameter, the perturbation is uniformly chosen from $[0, 1/(p - 1), \ldots, 1 - 1/(p - 1)]$, which implies that any parameter will have a variation within [-100% to +100%]. We utilize nine different optimal current profiles at three

TABLE II: Model parameters used in the Morris sensitivity method and their nominal value

Parameter(s)	Nominal Value(s)	Unit(s)
$R_{s,n}$	4.2642×10^{-6}	m
$D_{s,n}$	1.4493×10^{-14}	$m^2\,s^{-1}$
$\epsilon_{s,n}$	0.6187	-
k_n	1.0×10^{-10}	$m^{2.5}\,mol^{-0.5}\,s^{-1}$
κ_{sei}	17.5×10^{-5}	$S\,m^{-1}$
k_f	1.18×10^{-22}	-
ρ_{sei}	1690	$kg\,m^{-3}$

different ambient temperatures $T_{amb} = [15, 25, 35]°C$. Each profile is generated through a multi-objective fast charging-minimum degradation optimization problem defined as $\mathbf{U}^* = \mathrm{argmin}_{\mathbf{U}=[t_f, I_{cell}(t)]} \alpha_{OPT}\beta_1 t_f + \beta_2(1-\alpha_{OPT})(L_{sei}+\dot{L}_{sei})$ (from [20]), where the vector of optimization variables $\mathbf{U}^*$ is comprised of final time of charging t_f and the cell current I_{cell}; $\beta_1, \beta_2 > 0$ are the optimization weights; and $0 \leq \alpha_{OPT} \leq 1$ is a trade-off coefficient that can be adjusted for three different paradigms: fast charging ($\alpha_{OPT} = 1$), minimum degradation ($\alpha_{OPT} = 0$), and balanced charging-degradation ($\alpha_{OPT} = 0.5$). The operation of the battery cell requires solving the optimization subject to the battery cell dynamics and different task constraints [20] among which I_{app} must lie within the C-rate of 3C and 8C. Table III shows

TABLE III: Optimal Current Profiles

Scenario(s)	Profile	t_f (s)	T_{amb} (°C)
Minimum degradation	$I_{app,D1}$	393.1	15
	$I_{app,D2}$	668.3	25
	$I_{app,D3}$	716.9	35
Balanced	$I_{app,B1}$	389.8	15
	$I_{app,B2}$	538.6	25
	$I_{app,B3}$	713.4	35
Fast	$I_{app,F1}$	311	15
	$I_{app,F2}$	422.8	25
	$I_{app,F3}$	690	35

the three scenarios, and nine optimal profiles with final times t_f and corresponding ambient temperatures (see, Fig. 1).

A. Results

Morris' method is run for all nine optimal current profiles, and mean and standard deviation of all parameters are illustrated on a log-log plot. In Fig. 2, the heatmap shows the results of GSA for the cell voltage corresponding to different charging regimes. It can be seen that the least sensitive parameters are ρ_{sei}, k_f, and κ_{sei}. While the most sensitive
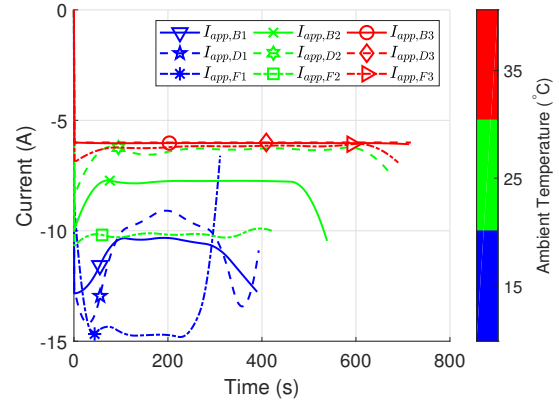
Fig. 1: Optimal input current profiles for balanced charging, fast charging-minimum degradation, and fast charging at $15°C$ (blue), $25°C$ (green), and $35°C$ (red).

parameters are $\epsilon_{s,n}$, k_n and $D_{s,n}$. As ambient temperature increases, the general trend of the parameters is to increase in both mean and standard deviation, which implies that sensitivity and non-linear interactions are generally larger at higher temperatures for the cell voltage. For cell capacity, since capacity change is a slow process and the effect of aging is not present in a fresh cell, the results are generated for a cell with an 8% capacity loss. This means that the cell has a high Ah-throughput implying that its capacity decreases over time. It can be seen in Fig. 3 that the same high sensitivity parameters for the cell voltage are also sensitive for the capacity. Furthermore, we see that k_f is another sensitive parameter for capacity which was not sensitive for cell voltage. This makes sense because k_f has a direct relation with the rate of change of capacity through i_s. Another interesting observation is that capacity is the least sensitive to ρ_{sei} at low temperature; however, as ambient temperature increases, capacity becomes relatively more sensitive to ρ_{sei} for all three optimal charging scenarios. Based on these results, the cell voltage with nominal value of parameters is compared with the one when the most ($\epsilon_{s,n}$ and k_n) and least (ρ_{sei}) sensitive parameters are perturbed by +33% (randomly selected from our set of perturbation intervals) from the nominal values at $T_{amb} = 25°C$ over fast charging-minimum degradation profile (see Fig. 5). This figure shows that due to the non-linear nature of the relationship between these parameters and cell voltage, it is not guaranteed that same direction of perturbation leads to similar changes in the voltage response. Hence, the focus is on the amount of perturbation, which is kept the same for all parameters. From Fig. 5, we can see that the perturbation in $\epsilon_{s,n}$ and k_n (most sensitive parameters) leads to a significant deviation from the voltage with nominal values. Fig. 5 also compares the error between the nominal voltage and the voltage when $\epsilon_{s,n}$, k_n, and ρ_{sei} are perturbed one-at-a-time. It can be seen that $\epsilon_{s,n}$ has the largest and ρ_{sei} has the smallest average error; this is consistent with what we observe from Fig. 2. A similar validation is performed for cell capacity using the same
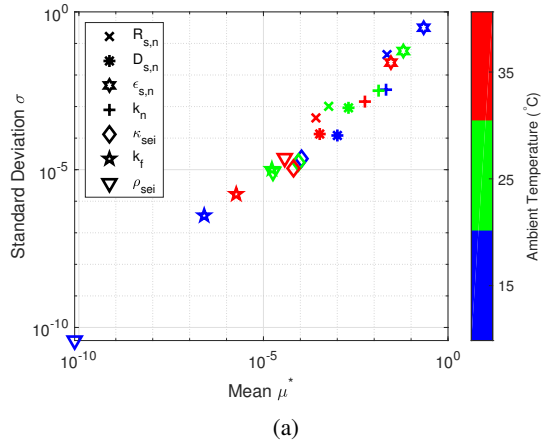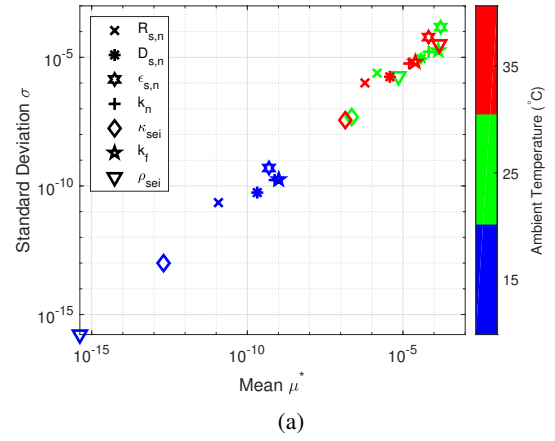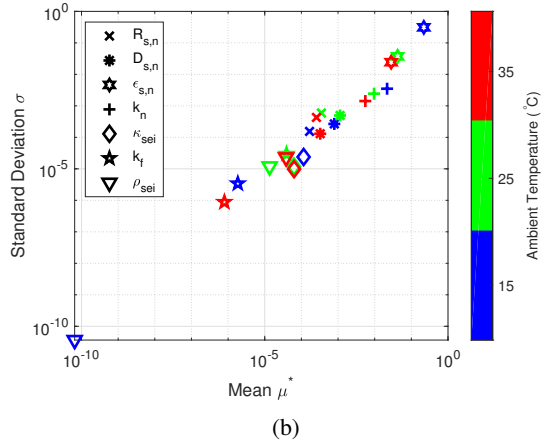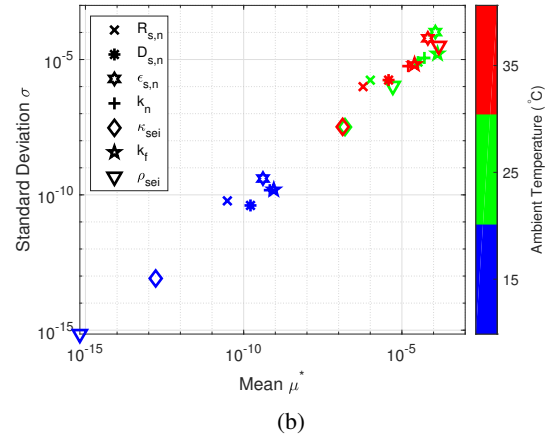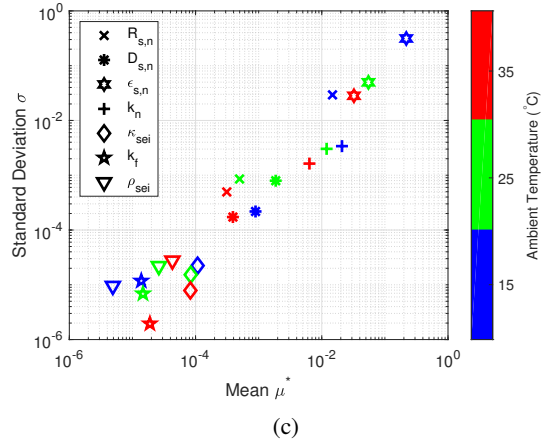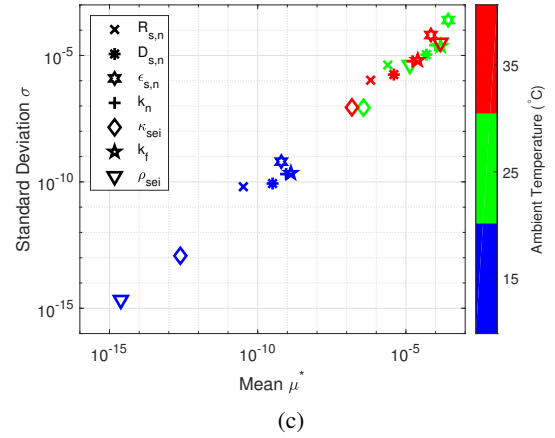
Fig. 2: Voltage heatmap of Morris' elementary effects for (a) balanced, (b) minimum-degradation, and (c) fast charging profiles for seven candidate parameters.

Fig. 3: Capacity heatmap of Morris' elementary effects for (a) balanced, (b) minimum-degradation, and (c) fast charging profiles for seven candidate parameters.

parameters and perturbation. The results of the validation are shown in the bar plots in Fig. 4. The reference bar shows the capacity loss for nominal values of the parameters. Perturbation in $\epsilon_{s,n}$ results in the largest capacity variation while perturbation in ρ_{sei} results in negligible variation in the output, which is consistent with the capacity sensitivity analysis shown earlier. Another interesting observation is that during fast charging, the degradation is relatively higher than

the other two charging scenarios.

IV. CONCLUSION

In this paper, a sensitivity technique was used to analyze and screen parameters a ESPM-thermal-aging model of LIB cell. Main focus of the sensitivity analysis was given to the aging parameters. Cell capacity and voltage were the considered outputs and different optimal current profiles to
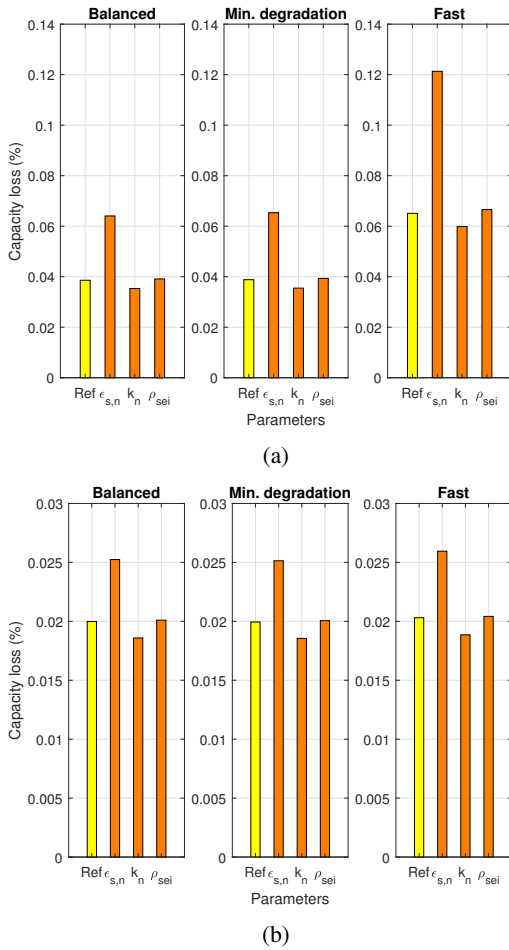
Fig. 4: Bar plots showing percentage capacity loss for all nine charging scenarios at a) 15^oC and and b) 35^oC. The results at 25^oC follow the same trends as the ones at 15^oC.
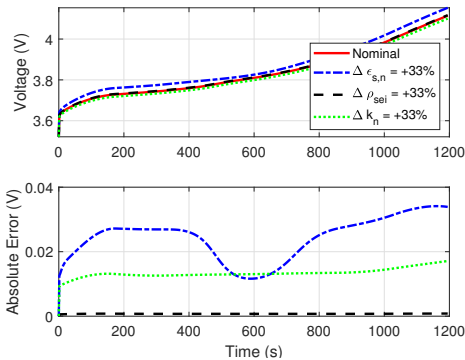
Fig. 5: The top figure shows the impact of perturbation of the most sensitive ($\epsilon_{s,n}$ and k_n), and least sensitive (ρ_{sei}) parameters on the cell voltage with fast charging-minimum degradation profile at $T_{amb} = 25°C$. The bottom figure shows the absolute error between cell voltage with one-at-a-time perturbed parameters and nominal voltage.

charge the cell at three ambient temperatures where used as case studies. Morris' method was used to conduct the

sensitivity analysis to explore how sensitive the selected outputs were to the aging parameters. The results revealed that the kinetic parameters are highly-sensitive while design and SEI parameters show low sensitivity for both the cell voltage and the capacity.

REFERENCES

[1] Sun, Kai, and Qifang Shu, "Overview of the types of battery models," Proceedings of the 30th Chinese Control Conference. IEEE, 2011.
[2] Doyle, Marc, Thomas F. Fuller, and John Newman, "Modeling of galvanostatic charge and discharge of the lithium/polymer/insertion cell," Journal of the Electrochemical society 140.6, 1993.
[3] Lai, X., Wang, S., Ma, S., Xie, J., & Zheng, Y, "Parameter sensitivity analysis and simplification of equivalent circuit model for the state of charge of lithium-ion batteries," Electrochimica Acta, 330, 2020.
[4] Zhou, X., & Huang, J, "Impedance-Based diagnosis of lithium ion batteries: Identification of physical parameters using multi-output relevance vector regression," Journal of Energy Storage, 31, 2020.
[5] Huang, H., Wang, H., Gu, J., & Wu, Y, "High-dimensional model representation-based global sensitivity analysis and the design of a novel thermal management system for lithium-ion batteries," Energy Conversion and Management, 190, 2019.
[6] Li, W., Cao, D., Jöst, D. et al., "Parameter sensitivity analysis of electrochemical model-based battery management systems for lithium-ion batteries," Applied Energy, 269, 2020.
[7] Jiang, K., Liu, X., Lou, G., Wen, Z., & Liu, L, "Parameter sensitivity analysis and cathode structure optimization of a non-aqueous Li–O2 battery model," Journal of Power Sources, 451, 2020.
[8] Edouard, C., Petit, M., Forgez, C., Bernard, J., & Revel, R, "Parameter sensitivity analysis of a simplified electrochemical and thermal model for Li-ion batteries aging," Journal of Power Sources, 325, 2016.
[9] Triantafyllidiis, V., Xing, W. W., Leung, P. K., Rodchanarowan, A., & Shah, A. A, "Probabilistic sensitivity analysis for multivariate model outputs with applications to Li-ion batteries," In Journal of Physics: Conference Series, 2018.
[10] Grandjean, T. R., Li, L., Odio, M. X., & Widanage, W. D, "Global Sensitivity Analysis of the Single Particle Lithium-Ion Battery Model with Electrolyte," IEEE VPPC, 2019.
[11] Pozzi, A., Xie, X., Raimondo, D. M., & Schenkendorf, R, "Global Sensitivity Methods for Design of Experiments in Lithium-ion Battery Context," arXiv preprint arXiv:2004.0966, 2020.
[12] T. R. Tanim, C. D. Rahn, and C.-Y. Wang, "A temperature dependent, single particle, lithium ion cell model including electrolyte diffusion," Journal of Dynamic Systems, Measurement, and Control, 2015.
[13] Y. Ji, Y. Zhang, and C.-Y. Wang, "Li-ion cell operation at low temperatures," Journal of The Electrochemical Society, 2013.
[14] E. Prada, D. Di Domenico, Y. Creff, J. Bernard, V. Sauvant-Moynot, and F. Huet, "A Simplified Electrochemical and Thermal Aging Model of LiFePO4-Graphite Li-ion Batteries: Power and Capacity Fade Simulations," Journal of The Electrochemical Society, 2013.
[15] X. Lin, H. E. Perez, S. Mohan, J. B. Siegel, A. G. Stefanopoulou, Y. Ding, and M. P. Castanier, "A lumped-parameter electro-thermal model for cylindrical batteries," Journal of Power Sources, 2014.
[16] M. Safari, M. Morcrette, A. Teyssot, and C. Delacourt, "Multimodal physics-based aging model for life prediction of li-ion batteries," J. of The Electrochemical Society, 2009.
[17] L. Valoen and J. Reimers, "Transport properties of lipf6-based li-ion battery electrolytes," J. of The Electrochemical Society, 2005.
[18] Morris, Max D, "Factorial sampling plans for preliminary computational experiments." Technometrics 33.2, 1991.
[19] C. D. Rahn and C.-Y. Wang, Battery systems engineering. John Wiley & Sons, 2013.
[20] V. Azimi, A. Allam, W. T. Joe, Y. Choi, S. Onori, "Fast charging-minimum degradation optimal control of series-connected battery modules with DC/DC bypass converters based on an electrochemical-thermal-aging model," American Control Conference, Accepted, 2021.
[21] A. Allam and S. Onori, "Online Capacity Estimation for Lithium-Ion Battery Cells via an Electrochemical Model-Based Adaptive Interconnected Observer," in IEEE Transactions on Control Systems Technology, vol. 29, no. 4, pp. 1636-1651, July 2021.
[22] A. Allam and S. Onori, "An Interconnected Observer for Concurrent Estimation of Bulk and Surface Concentration in Cathode and Anode of a Lithium-ion Battery," in IEEE Transactions on Industrial Electronics, vol. 65, no. 9, 2018.